Automated Assessment of Aortic and Main Pulmonary Arterial Diameters using Model-Based Blood Vessel Segmentation for Predicting Chronic Thromboembolic Pulmonary Hypertension in Low-Dose CT Lung Screening

Hidenobu Suzuki *[a], Yoshiki Kawata [a], Noboru Niki [a],
Toshihiko Sugiura [b], Nobuhiro Tanabe [b], Masahiko Kusumoto [c], Kenji Eguchi [d], Masahiro Kaneko [e]

[a] Department of optical Science, Tokushima University, Tokushima, Japan; [b] Department of Respirology, Chiba University, Chiba, Japan; [c] Division of Diagnostic Radiology, National Cancer Center Hospital East, Chiba, Japan; [d] Health Science on Supportive Medicine for Intractable Diseases, Teikyo University, Tokyo, Japan; [e] Tokyo Health Service Association, Tokyo, Japan

ABSTRACT

Chronic thromboembolic pulmonary hypertension (CTEPH) is characterized by obstruction of the pulmonary vasculature by residual organized thrombi. A morphological abnormality inside mediastinum of CTEPH patient is enlargement of pulmonary artery. This paper presents an automated assessment of aortic and main pulmonary arterial diameters for predicting CTEPH in low-dose CT lung screening. The distinctive feature of our method is to segment aorta and main pulmonary artery using both of prior probability and vascular direction which were estimated from mediastinal vascular region using principal curvatures of four-dimensional hyper surface. The method was applied to two datasets, 64 low-dose CT scans of lung cancer screening and 19 normal-dose CT scans of CTEPH patients through the training phase with 121 low-dose CT scans. This paper demonstrates effectiveness of our method for predicting CTEPH in low-dose CT screening.

Keywords: Chronic thromboembolic pulmonary hypertension, computed tomography, computer aided diagnosis, CT lung screening

1. INTRODUCTION

Chronic thromboembolic pulmonary hypertension (CTEPH) is characterized by obstruction of the pulmonary vasculature by residual organized thrombi [1][2]. Patients with CTEPH have a poor prognosis unless they receive early treatment [2]. A morphological abnormality inside mediastinum of CTEPH patient is enlargement of pulmonary artery. The diameters of mediastinal blood vessels are effective biomarkers for pulmonary hypertension diagnosis [3]-[7]. The vascular boundaries in the contrast-enhanced CT images are clear without complex vascular contacts. However, CT screening for detecting the thoracic diseases in the early stage have been performed without the contrast materials. In addition, the contrast agent injection cannot be used with participants who are allergic to these agents. The purpose of this study is to develop an automated assessment method of aortic and main pulmonary arterial diameters using model-based blood vessel segmentation for predicting CTEPH in low-dose CT lung screening.

Many automated segmentation methods of the aorta and main pulmonary artery were proposed [8]-[19]. Previous automated methods are classified into three groups based on the modalities used, i.e., contrast enhanced computed tomography (CT) approaches [8]-[10], non-contrast CT approaches [11]-[17], and magnetic resonance approaches [18],[19]. Some solutions for aorta or main pulmonary artery segmentation on non-contrast CT images have been proposed. In this work, we propose an automated assessment method of aortic and main pulmonary arterial diameters using model-based blood vessel segmentation. Our method comprises training and testing phases. In the training phase, we constructed probabilistic atlases of the aorta and main pulmonary artery centerlines that were extracted from initial region of mediastinal blood vessel. In the testing phase, we used the mediastinal vascular centerlines and the probabilistic atlases to segment the aorta and main pulmonary artery. The diameters of the ascending aorta and

Medical Imaging 2018: Computer-Aided Diagnosis, edited by Nicholas Petrick, Kensaku Mori, Proc. of SPIE Vol. 10575, 105750X · © 2018 SPIE · CCC code: 1605-7422/18/$18 · doi: 10.1117/12.2293295

pulmonary trunk were measured. The method was applied to two datasets, 64 low-dose CT scans of lung cancer screening and 19 normal-dose CT scans of CTEPH patients after a training phase with 121 low-dose CT scans. This paper demonstrates that the proposed method achieves high performance and that the method is useful for statistical diagnosis of CTEPH.

2. MATERIALS AND METHODS

2.1 Datasets

This study collected three CT datasets from two medical institutions. Collection and analysis of data were approved by the Institutional Review Board at each institution. The personal information in the DICOM header information was anonymized by our DICOM anonymization system [20]. First and second datasets are 121 scans (dataset A) and 64 scans (dataset B) that were collected from low-dose CT lung screening in Tokyo Health Service Association. Figure 1 shows the example of mediastinal blood vessels on non-contrast CT images. These data were acquired on Aquilion scanner with 30 mA at 120 kVp, plane resolution: 0.625 or 0.781 mm, reconstruction matrix: 512 x 512, convolution kernel: FC01, slice thickness: 1.0 mm, and reconstruction interval: 1.0 mm. Mean and standard deviation (SD) of participant age in dataset A and B were 62.3±10.0 and 68.0±10.8 years respectively. Third dataset is 19 scans of CTEPH patients that were collected from Chiba University Hospital (dataset C). These data were acquired on Aquilion scanner with 112 to 295 mA at 120 kVp, plane resolution: 0.570 to 0.698 mm, reconstruction matrix: 512 x 512, convolution kernel: FC07, slice thickness: 0.5 mm, reconstruction interval: 0.5 mm. Mean and SD of patient age were 64.6±6.9 years.

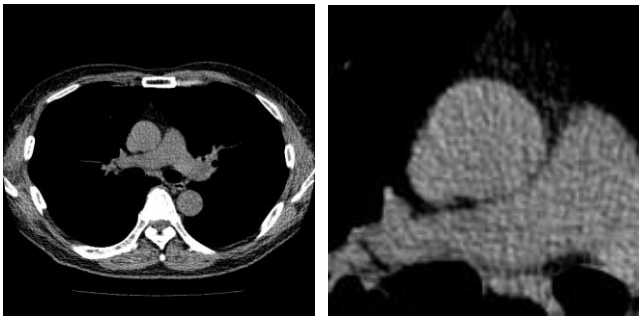

(A) (B)

Figure 1. An example of mediastinal blood vessels on non-contrast CT images. (A) Original CT slice, and (B) magnified CT slice. The window center and width are 50 HU and 300 HU, respectively.

An observer determined the ground truth of the aorta and main pulmonary artery separately in the axial plane. The vertical interval of the manual segmentation is 10 slices. The ground truth was observed with a mediastinal window setting that had a window width and center set to 300 HU and 50 HU, respectively. The observer carried out the manual segmentations of the all scans in datasets B and C once.

2.2 Model-based segmentation of aorta and main pulmonary artery

Our framework is shown in Figure 2. The training phase consisted of initial region segmentation of mediastinal blood vessel, mediastinal vascular centerlines extraction, and probabilistic atlas constructions of the aorta and main pulmonary artery centerlines. The testing phase consisted of initial region segmentation of mediastinal blood vessel, mediastinal vascular centerlines extraction, aorta and main pulmonary artery segmentation, and three-dimensional measurements of the aorta and main pulmonary artery diameters.

1) Initial region segmentation of mediastinal blood vessel

This method was employed as the first process in the training and testing phases. All data were smoothed by bilateral filtering (σ_c=1.0, σ_r=30 HU) [21]. Body, bone, lungs, and airway were segmented using our previously proposed methods based on intensity and anatomical features [22],[23]. The mediastinum was segmented from the body tissue region using the thoracic cavity surface [24]. The CT value histogram in the mediastinum had a bimodal distribution. The CT value histogram was divided into two classes using the Gaussian mixture model classification. A class with the highest peak frequency was identified as the initial region of mediastinal blood vessel.

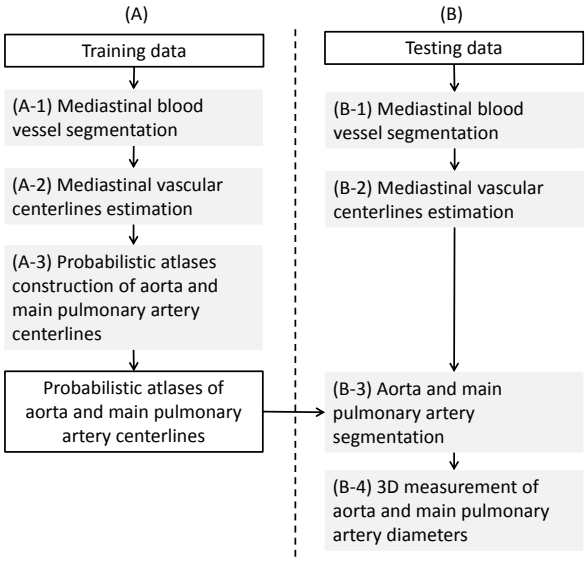

Figure 2. Our framework for automated assessment of aortic and main pulmonary arterial diameters. (A) Training phase, and (B) testing phase. White and gray boxes represent data and processing, respectively.

2) Mediastinal vascular centerlines extraction

Mediastinal vascular centerlines were extracted from the initial region of mediastinal blood vessel in two steps. The first step is principal curvatures calculation of four-dimensional hyper surface. Binary images of the initial region of mediastinal blood vessel were converted to gray-level images using three-dimensional Euclidean distance transform. A vector of principal curvatures $\boldsymbol{k} = (k_1, k_2, k_3)$ on each voxel was calculated from the gray-level images using the principal curvaturse of four-dimensional hyper surface [25],[26]. The second step is curvature-based vascular centerlines extraction. The method extracted the vascular centerlines based on two features, line similarity and vascular direction similarity which were calculated from the principal curvatures.

3) Probabilistic atlas constructions of the aorta and main pulmonary artery centerlines

Aorta and main pulmonary artery centerlines in training data were selected and refined by an observer semi-automatically. Probabilistic atlases for aorta and main pulmonary artery centerlines were created from training data by following steps; morphological dilation of centerlines, spatial normalization using bounding box for lungs, standard probability model construction, and principal component analysis. The standard probability models of aorta and main pulmonary artery centerlines were obtained by averaging of the all spatial normalized data. Principal components of aorta and main pulmonary artery centerlines were obtained by principal component analysis. In this study, five principal components of aorta centerlines and two principal components of main pulmonary artery centerlines which are over 0.8 in cumulative contribution ratio were employed.

4) Aorta and main pulmonary artery segmentation

The aorta and main pulmonary artery centerlines on an input scan were selected from mediastinal vascular centerlines using the probabilistic atlases. An optimal probabilistic atlas Z for an input scan was given by $Z = Z_\mu + w_1\sigma_1 Z_1 + w_2\sigma_2 Z_2 + \ldots + w_n\sigma_n Z_n$ where Z_μ is a standard probability model, n is the number of principal components, Z_n is a principal component, σ_n is the standard deviation of the principal component, and w_n is the constant value to weight the principal component. The weight parameters $\boldsymbol{w} = \{w_1, w_2, \ldots, w_n\}$ were optimized by a cost function which is defined by the prior probability and vascular direction calculated from the probabilistic atlas. Local optimal solution of the cost function with weight parameters $\boldsymbol{w}$ is found out by Quasi-Newton method.

2.3 Assessment of aortic and main pulmonary arterial diameters

Thinning lines of aorta and main pulmonary artery were derived by a thinning method based on Euclidean distance transform. Thinning line of main pulmonary artery was divided into three lines, pulmonary trunk, right main pulmonary artery, and left main pulmonary artery. Lines with 20 mm length were selected from the thinning lines of ascending aorta

and pulmonary trunk. Volumes of interest (VOI) along the lines were segmented from aorta and main pulmonary artery regions using surfaces perpendicular to the lines on begin and end points. Vascular diameters were estimated from the VOIs.

3. RESULTS

Examples of the aorta and main pulmonary artery segmentation result from datasets B and C are shown in Figure 3. Performance of segmentation was evaluated according to two metrics, Jaccard coefficient and Dice coefficient. Performances of the aorta and main pulmonary artery segmentation are shown in Tables I and II, respectively.

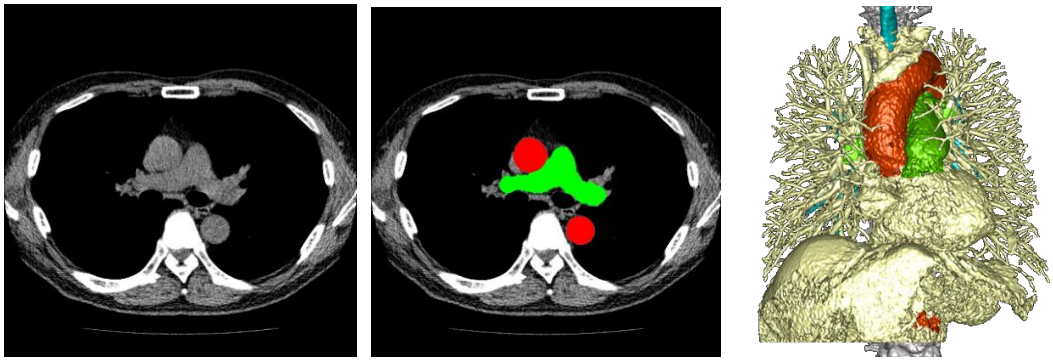

(A) (B) (C)

Figure 3. Segmentation results of the aorta and main pulmonary artery. (A) and (B) are the CT image and a segmentation result from dataset B. Red and green regions are the aorta and main pulmonary artery, respectively.

Table 1. Performances of aorta segmentation

	Dataset B	Dataset C
Jaccard coefficient	0.916±0.013	0.911±0.023
Dice coefficient	0.956±0.007	0.953±0.012

Table 2. Performances of main pulmonary artery segmentation

	Dataset B	Dataset C
Jaccard coefficient	0.902±0.019	0.914±0.017
Dice coefficient	0.948±0.009	0.955±0.009

Diameter measurement results are shown in Figure 4. In dataset B, mean diameters and SD of aorta and pulmonary trunk were 3.219±0.297 and 2.360±0.223 cm respectively. In dataset C, mean diameters and SD of aorta and pulmonary trunk were 3.124±0.333 and 3.220±0.486 cm respectively. These diameters in the two datasets were compared by Welch's t-test. There was no significant difference in aorta diameters (p-value=0.275). Pulmonary trunk diameter in dataset C was significantly larger than the diameter in dataset B (p-values=2.96×10^{-7}).

4. CONCLUSIONS

We presented an automated assessment method of aortic and main pulmonary arterial diameters using model-based blood vessel segmentation for predicting CTEPH in low-dose CT lung screening. The method was applied to two datasets: 64 low-dose CT scans of lung cancer screening and 19 normal-dose CT scans of CTEPH patients after a training phase with 121 low-dose CT scans. Dice coefficients of aorta segmentation in low-dose and normal-dose CT scans were 0.956±0.007 and 0.953±0.012, respectively. The dice coefficients of the pulmonary trunk and main pulmonary arteries segmentation in low-dose CT scans and normal-dose CT scans were 0.948±0.009 and 0.955±0.009, respectively. The application of the method could lead to the quantitative CTEPH diagnosis in non-contrast low-dose CT screening.

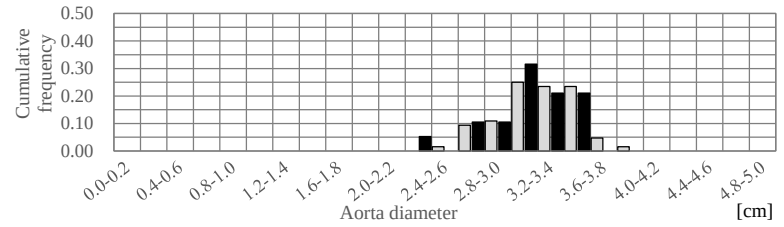

(A)

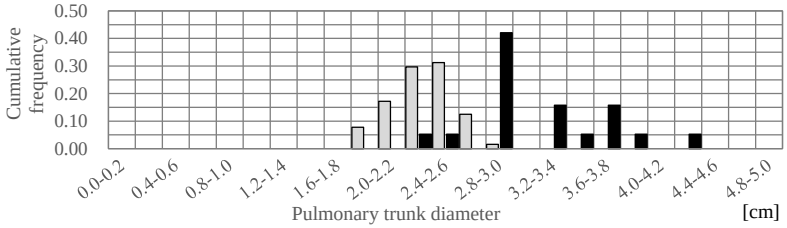

(B)

Figure 4. Cumulative frequency of vascular diameters. The diameter histograms of the aorta and pulmonary trunk are presented in (A) and (B), respectively. Gray and black bars are the diameters that were measured from dataset B and dataset C.

ACKNOWLEDGEMENT

This work was supported by a JSPS Grant-in-Aid for Scientific Research on Innovative Areas (Multidisciplinary Computational Anatomy) JSPS KAKENHI Grant Number 26108007, and by the Terumo Foundation for Life Science and Arts.

REFERENCES

[1] Wilkens, H. Lang, I. Behr, J. Berghaus, T. Grohe, C. Guth, S. Hoeper, M. M. Kramm, T. Krüger, U. Langer, F. Rosenkranz, S. Schäfers, H. Schmidt, M. Seyfarth, H. Wahlers, T. Worth, H. and Mayer, E., "Chronic thromboembolic pulmonary hypertension (CTEPH): Updated recommendations of the cologne consensus conference 2011, " Int. J. Cardiol. 154(1), s54-s60 (2011)

[2] Ghofrani, H. A. D'armini, A. M. Grimminger, F. Hoeper, M. M. Jansa, P. Kim, N. H. Mayer, E. Simonneau, G. Wilkins, M. R. Fritsch, A. Neuser, D. Weimann, G. and Wang C., "Riociguat for the treatment of chronic thromboembolic pulmonary hypertension," N. Eng. J. Med. 369(4), 319-329 (2013)

[3] Kuriyama, K. Gamsu, G. Stern, R. G. Cann, C. E. Herfkens, R. J and Brundage B. H., "CT-Determined Pulmonary Artery Diameters in Predicting Pulmonary Hypertension," Investigative Radiology 19(1), 16-22 (1984)

[4] Edwards, P. D. Bull, R. K. and Coulden, R., "CT measurement of main pulmonary artery diameter," Br. J. Radiol. 71(850), 1018-1020 (1998)

[5] Truong, Q. A. Massaro, J. M. Rogers, I. S. Mahabadi A. A., Kriegel, M. F. Fox, C. S. O'Donnell, C. J. and Hoffmann U., "Reference Values for Normal Pulmonary Artery Dimensions by Noncontrast Cardiac Computed Tomography, The Framingham Heart Study," Circ. Cardiovasc. Imaging 5(1), 147-154 (2012)

[6] Corson, N. Armato III S. G., Labby, Z. E. Straus, C. Starkey, A. and Gomberg-Maitland M., "CT-Based Pulmonary Artery Measurements for the Assessment of Pulmonary Hypertension," Acad. Radiol. 21(4), 523-530 (2014)

[7] Spruijt, O. A. Bogaard, H. Heijmans, M. W. Lely, R. J. van de Veerdonk, M. C. de Man, F. S. Westerhof, N. and Vonk-Noordegraaf, A. "Predicting pulmonary hypertension with standard computed tomography pulmonary angiography," Int. J. Cardiovasc. Imaging 31(4), 871-879 (2015)

[8] Vitanovski, D. Ionasec, R. I. Georgescu, B. Huber, M. Taylor, A. M. Hornegger, J. and Comaniciu, D. "Personalized pulmonary trunk modeling for intervention planning and valve assessment estimated from CT data," in Int. Conf. Med. Image. Comput. Comput. Assist. Interv. 5761, 17-25 (2009)
[9] Linguraru, M. G. Pura, J. A. Van Uitert R. L., Mukherjee, N. Summers, R. M. Minniti, C. Gladwin, M. T. Kato, G. Machado, R. F. and Wood, B. J. "Segmentation and quantification of pulmonary artery for noninvasive CT assessment of sickle cell secondary pulmonary hypertension," Med. Phys. 37(4), 1522-1532 (2010)
[10] Biesdorf, A. Rohr, K. Feng, D. von Tengg-Kobligk, H. Rengier, F. Böckler, D. Kauczor, H. and Wörz, S. "Segmentation and quantification of the aortic arch using joint 3D model-based segmentation and elastic image registration," Medical Image Analysis 16(6), 1187-1201 (2012)
[11] Moses, D. Sammut, C. and Zrimec, T. "Automatic segmentation and analysis of the main pulmonary artery on standard post-contrast CT studies using iterative erosion and dilation," Int. J. CARS 11(3), 381-395 (2016)
[12] Išgum, I. Staring, M. Rutten, A. Prokop, M. Viergever, M. A. and van Ginneken, B. "Multi-Atlas-Based Segmentation With Local Decision Fusion—Application to Cardiac and Aortic Segmentation in CT Scans," IEEE Trans. Med. Imaging 28(7), 1000-1010 (2009)
[13] Išgum, I. Rutten, A. Prokop, M. Saring, M. Klein, S. Pluim, J. P. W. Viergever, M. A. and van Ginneken, B. "Automated aortic calcium scoring on low‐dose chest computed tomography," Med. Phys. 37(2), 714-723 (2010)
[14] Kurugol, S. Estepar, R. S. J. Ross, J. and Washko, G. R. "Aorta segmentation with a 3D level set approach and quantification of aortic calcifications in non-contrast chest CT," in Annual Int. Conf. of the IEEE, 2343-2346 (2012)
[15] Kurugol, S. Come, C. E. Diaz, A. A. Ross, J. C. Kinney, G. L. Black-shinn, J. L. Hokanson, J. E. Budoff, M. J. Washko, G. R. and Estepar, R. S. J. "Automated quantitative 3D analysis of aorta size, morphology, and mural calcification distributions," Med. Phys. 42(9), 5467-5478 (2015)
[16] Xie, Y. Padgett, J. Biancardi, A. M. and Reeves, A. P. "Automated aorta segmentation in low-dose chest CT images," Int. J. CARS 9(2), 211-219 (2014)
[17] Xie, Y. Liang, M. Yankelevitz, D. F. Henschke, C. I. and Reeves, A. P. "Automated measurement of pulmonary artery in low-dose non-contrast chest CT images," Proc. SPIE 9414, 9414G (2015)
[18] Rueckert, D. Burger, P. Forbat, S. M. Mohiaddin, R. D. and Yang, G. Z. "Automatic tracking of the aorta in cardiovascular MR images using deformable models," IEEE Trans. Med. Imaging 16(5), 581-590 (1997)
[19] Rengier, F. Wörz, S. Melzig, C. Ley, S. Fink, C. Benjamin, N. Partovi, S. von Tengg-Kobligk, H. Rohr, K. Kauczor, H. and Grünig, E. "Automated 3D Volumetry of the Pulmonary Arteries based on Magnetic Resonance Angiography Has Potential for Predicting Pulmonary Hypertension," PLoS ONE 11(9), e0162516 (2016)
[20] Suzuki, H. Amano, M. Kubo, M. Kawata, Y. Niki, N. and Nishitani, H. "Anonymization server system for DICOM images," Proc. SPIE 6516, 65160Z (2007)
[21] Tomasi, C. and Manduchi, R. "Bilateral filtering for gray and color images," Proc. Sixth Int. J. Conf. Computer Vision, 839-846 (1998)
[22] Kanazawa, K. Kawata, Y. Niki, N. Satoh, H. Ohmatsu, H. Kakinuma, R. Kaneko, M. Moriyama, N. and Eguchi, K. "Computer-aided diagnosis for pulmonary nodules based on helical CT images," Comput. Med. Imaging Graph. 22(2), 157-167 (1998)
[23] Yoneda, K. Matsuhiro, M. Suzuki, H. Kawata, Y. Niki, N. Nakano, Y. Ohmatsu, H. Kusumoto, M. Tsuchida, T. Eguchi, K. Kaneko, M. "Computer-aided diagnosis for osteoporosis using chest 3D CT images," Proc. of SPIE 9785, 97853A (2016)
[24] Matsuhiro, M. Suzuki, H. Kawata, Y. Niki, N. Nakano, Y. Ohmatsu, H. Kusumoto, M. Tsuchida, T. Eguchi, K. Kaneko, M. "Peripleural lung disease detection based on multi-slice CT images," Proc. of SPIE, 9414, 94142W (2015)
[25] Monga O. and Benayoun, S. "Using partial derivatives of 3D images to extract typical surface features," Comput. Vis. Image underst. 61(2), 171-189 (1995)
[26] Kawata, Y. Kubo, H. Niki, N. Ohmatsu, H. and Moriyama, N. "A study of three-dimensional curvatures and curvatures of four-dimensional hypersurface for analyzing pulmonary nodules on high-resolution CT images," Systems and Computers in Japan 36(10), 16-29 (2005)